Enhancement and wavelength-shifted emission of Cerenkov luminescence using multifunctional microspheres

Joanne Li[1,2,3], **Lawrence W Dobrucki**[1,3], **Marina Marjanovic**[1,3], **Eric J Chaney**[1], **Kenneth S Suslick**[1,4] **and Stephen A Boppart**[1,2,3,5,6]

[1] Beckman Institute for Advanced Science and Technology, University of Illinois at Urbana-Champaign, Urbana, IL, USA
[2] Department of Nuclear, Plasma, and Radiological Engineering, University of Illinois at Urbana-Champaign, Urbana, IL, USA
[3] Department of Bioengineering, University of Illinois at Urbana-Champaign, Urbana, IL, USA
[4] Department of Chemistry, University of Illinois at Urbana-Champaign, Urbana, IL, USA
[5] Department of Electrical and Computer Engineering, University of Illinois at Urbana-Champaign, Urbana, IL, USA
[6] Department of Internal Medicine, University of Illinois at Urbana-Champaign, Urbana, IL, USA

E-mail: boppart@illinois.edu

Abstract

Cerenkov luminescence (CL) imaging is a new molecular imaging modality that utilizes the photons emitted during radioactive decay when charged particles travel faster than the phase velocity of light in a dielectric medium. Here we present a novel agent to convert and increase CL emission at longer wavelengths using multimodal protein microspheres (MSs). The ^{64}Cu-labeled protein microspheres contain quantum dots (QDs) encapsulated within a high-refractive-index-oil core. Dark box imaging of the MSs was conducted to demonstrate the improvement in CL emission at longer wavelengths. To illustrate the versatile design of these MSs and the potential of CL in disease diagnosis, these MSs were utilized for *in vitro* cell targeting and *ex vivo* CL-excited QD fluorescence (CL-FL) imaging of atherosclerotic plaques in rats. It was shown that by utilizing both QDs and MSs with a high-refractive-index-oil core, the CL emission increases by four-fold at longer wavelengths. Furthermore, we demonstrate that these MSs generate both an *in vivo* and *ex vivo* contrast signal. The design

concept of utilizing QDs and high-index core MSs may contribute to future developments of *in vivo* CL imaging.

S Online supplementary data available from stacks.iop.org/PMB/60/020727/mmedia

(Some figures may appear in colour only in the online journal)

1. Introduction

Molecular imaging has become an indispensable tool in biomedical research by providing spatially-resolved molecular information for drug development and diagnosis of various diseases (Weissleder and Pittet 2008, Xu *et al* 2011). Nuclear imaging techniques, such as PET and SPECT, have been shown to provide valuable information in both the research and the clinical settings (Dobrucki and Sinusas 2010, Thorek *et al* 2012). A recent development has been the ability to optically visualize radioactive decay signals from medical isotopes, known as Cerenkov luminescence (CL) imaging (Robertson *et al* 2009, Ruggiero *et al* 2010). Cerenkov luminescence imaging may offer relatively lower cost molecular imaging capabilities for screening applications, compared to PET and SPECT, and has the potential for bridging the information acquired from nuclear and optical imaging.

Cerenkov luminescence imaging utilizes the principle of Cerenkov radiation generation (Mitchell *et al* 2011), which is analogous to the sonic boom phenomenon. During Cerenkov radiation, the electron distribution in the medium is disrupted as the charged particle travels through the medium and loses kinetic energy by polarizing surrounding electrons (Ruggiero *et al* 2010). These polarized molecules re-equilibrate through emission of ultra violet (UV) and visible light when the speed of the charged particle exceeds the phase velocity of light, giving the observed CL (Robertson *et al* 2009, Ruggiero *et al* 2010, Mitchell *et al* 2011). Unlike fluorescence emission, CL emission is directional, with a continuous and broad spectrum that extends from the UV to the near-infrared (NIR) (Ruggiero *et al* 2010, Mitchell *et al* 2011). The production of CL can be described by the Frank-Tamm formula (Mitchell *et al* 2011):

$$\frac{\mathrm{d}N}{\mathrm{d}x} = 2\pi\alpha \left(1 - \frac{1}{\beta^2 n^2}\right) \int_{\lambda_1}^{\lambda_2} \frac{1}{\lambda^2} \mathrm{d}\lambda \tag{1}$$

where $\mathrm{d}N/\mathrm{d}x$ is the number of photons generated per distance, α is the dimensionless fine-structure constant (1/137), n is the refractive index of the medium, and β is the ratio of particle velocity to the speed of light (v/c) (Mitchell *et al* 2011). Equation (1) shows that CL emission is inversely proportional to the square of the wavelength (λ), indicating CL emission is greater at shorter wavelengths (Jelley 1955, Robertson *et al* 2009, Ruggiero *et al* 2010, Mitchell *et al* 2011). In addition, the intensity of CL generated in materials increases with higher refractive index (Robertson *et al* 2009, Mitchell *et al* 2011). This can be explained by considering the relationship between refractive index and the minimum threshold energy at which CL light may be emitted. Since the phase velocity of light decreases with increasing refractive index, the minimum threshold kinetic energy for the particles therefore decreases, and results in higher production of CL light (Jelley 1955).

The concept of CL imaging was demonstrated in the pre-clinical setting using a sensitive charged-couple device (CCD) camera to detect CL generated from β-emitting (both electrons

and positrons) isotopes (Robertson *et al* 2009). Furthermore, several research groups independently showed the feasibility of utilizing CL imaging for disease targeting and drug tracking in small animals (Mitchell *et al* 2011, Liu *et al* 2012, Xu *et al* 2012). However, one primary limitation of using CL in biomedical imaging is its short-wavelength emission, which is strongly absorbed by biological chromophores such as hemoglobin and melanin (Boschi and Spinelli 2012), making CL imaging of deeper tissues challenging. To overcome this limitation, it has been proposed that quantum dots (QDs) could serve as a suitable CL conversion agent due to their broad continuous UV-blue absorption spectrum which overlaps with the emission spectrum of CL, their high quantum efficiency, and large Stokes shift (Wu *et al* 2003, Smith *et al* 2008, Dothager *et al* 2010, Liu *et al* 2010, Boschi and Spinelli 2012). This spectral shift phenomenon was previously characterized as Cerenkov radiation energy transfer (CRET) (Dothager *et al* 2010). To use CL to excite a fluorescent agent and generate an emission in the longer-wavelength region, the absorption and emission spectra of the fluorescent agent need to be well separated. Since QDs have a large Stokes shift, they can be readily excited by CL, and the resulting optical emission can be shifted to longer wavelengths which are more suitable for deep-tissue imaging (Dothager *et al* 2010, Liu *et al* 2010).

Since the output of CL increases with higher refractive index (Mitchell *et al* 2011), CL emission can potentially be further increased by utilizing protein-shell microspheres (MSs) that contain a high-refractive-index core. These MSs consist of a vegetable oil core and a hydrophilic shell made of cross-linked bovine serum albumin (BSA) subunits (Toublan *et al* 2006). In this study, we encapsulated QDs in MSs that have a high-refractive-index-oil core to increase CL, and rely on the QDs to wavelength-shift the emission into the NIR. Furthermore, we utilized these MSs for targeting atherosclerotic lesions as a proof-of-concept study to demonstrate the versatile design of these MSs as a targeted contrast agent with the potential for biomedical imaging.

2. Materials and methods

2.1. Quantum dot microsphere preparation

The QD stock solution with an 800 nm emission peak (Qdot 800 ITK organic quantum dots, 1μM in decane, 4 mL solution, Invitrogen) received from the manufacturer was mixed with four times the volume of isopropanol/methanol mixture (75/25 volume ratio) in a sealed test tube. The mixture was then centrifuged at 3000 rpm for 5 min to separate the QDs and the solvent. The supernatant fluid (decane and isopropanol/methanol solvent) was removed, and the QDs were re-suspended in 1 mL of vegetable oil. Each batch of MSs was composed of 4 mL of 5% BSA solution and 1 mL of the QD-oil suspension. The process of encapsulating the QD-oil suspension within the BSA shell was mediated through sonication, utilizing high-frequency ultrasound (20 kHz) delivered by a 1 cm diameter acoustic horn at an acoustic power of 35 W cm^{-2} for 3 min (John *et al* 2012). During the process, the BSA protein subunits cross-linked through sonochemical formation of disulfide bonds via inter protein cysteine oxidation (Toublan *et al* 2006, John *et al* 2012). Following sonication, the MS emulsion was repeatedly washed with cold 5% BSA solution and centrifuged at 5000 rpm for 3 min to remove excess reagents.

2.2. Targeted microsphere surface modification

Before use, MSs were first centrifuged and washed with 1 × PBS at pH 8 to remove excess BSA. To ensure longer circulation time, MSs were PEGylated. The PEG reagent, (N-hydroxysuccinimide)-(polyethylene glycol)$_{5k}$-maleimide (NHS-PEG$_{5k}$-MAL, JenKem,

U.S.A.), was prepared by dissolving the compound in anhydrous dimethylformamide (DMF, Sigma-Aldrich). The concentration of MSs was first determined using the Lowry assay (Peterson 1977), and the PEG reagent was then mixed at a 5:1 (PEG/BSA) ratio with the MSs suspended in PBS. The mixture was rotated for one hour to allow the PEG agent to covalently bind to the amine on the BSA shell of the MSs. Afterward, MSs were centrifuged at 5000 rpm for 3 min to remove the unlabeled reagent. The PEGylated MSs were subsequently re-suspended in $1 \times$ PBS solution at pH 7.4.

To target the $\alpha_v\beta_3$ integrin overexpressed on atherosclerotic lesions (Hoshiga *et al* 1995, Winter *et al* 2003, Burtea *et al* 2008), the PEGylated MSs were functionalized with the cyclic RGD peptide (cRGD). The cyclo (Arg-Gly-Asp-D-Phe-Cys) (cRGDfc, Peptide International) compound was first activated using a *tris* (2-carboxyethyl) phosphine reducing agent (TCEP, Sigma-Aldrich) in $1 \times$ PBS solution at pH 7.4. After activation, the cRGD solution was combined with the PEGylated MS suspension. The mixture was subsequently rotated for 30 min at room temperature to allow binding between the thiol groups on the cRGD and the maleimide groups on the PEG. Cyclic RGD-functionalized PEGylated MSs were then centrifuged and washed to remove excess reagents and re-suspended in $1 \times$ PBS solution at pH 7.4.

2.3. Non-targeted microsphere surface modification

The non-targeted MSs were PEGylated using the NHS-PEG$_{5k}$-CH$_3$ (JenKem, U.S.A.) compound, which is PEG with methyl groups at the terminal end instead of maleimide groups. The PEGylation procedure was identical to that described previously for the targeted MSs. Cyclic RGD functionalization was not performed after the PEGylation step.

2.4. Copper-64 isotope labeling

A solution of $^{64}CuCl_2$ in ammonium acetate (Washington University, St. Louis, MO) containing the Copper-64 (^{64}Cu, $t_{1/2} = 12.7$ h) radioactive isotope was incubated with the surface-modified MSs for one hour at 28 °C. After the incubation, the MS suspension was washed with PBS and centrifuged in centrifuge tube filters to remove unlabeled isotope. The labeled MSs were re-suspended in $1 \times$ PBS solution at pH 7.4. The stability of ^{64}Cu labeling was evaluated using thin-layer chromatography (TLC), and more than 95% of the MSs remained labeled after 24 h.

2.5. In vitro cell targeting

Human breast cancer cell lines, MDA-MB-231 and MCF-7, were acquired from ATCC (Manassas, VA), and the human umbilical vein endothelial cell line (HUVEC) was purchased from Lonza (Lonza Group, Ltd, Switzerland). Cells were seeded and prepared 24 hrs prior the experiment. Before introducing the MSs, the cell media in each culture dish was aspirated and fresh media was added to the culture dish. The cells were then incubated with $100 \mu L$ of 2 mM manganese solution in PBS for 10 min to activate the $\alpha_v\beta_3$ integrins (Jackson *et al* 1997). After activation, MSs were added to the cells (10^4 MSs/cell dish) and allowed to incubate for one hour. Prior to fluorescence microscopy, all cell samples were washed using $1 \times$ PBS to remove any dead cells and excess MSs.

2.6. Animals

Animals were cared for in accordance with a protocol approved by the University of Illinois at Urbana-Champaign Institutional Animal Care and Use Committee (IACUC). To compare

the difference in optical intensity between CL and CL-FL in tissue, equal doses and volumes of ^{64}Cu isotope and ^{64}Cu-labeled QD-MSs were subcutaneously injected at different skin locations in a previously sacrificed C57/BL6 mouse. The mouse was then imaged using the luminescence dark box system (Stanford Photonics, Palo Alto, CA).

For *in vivo* atherosclerotic lesion targeting, Wistar-Furth rats were fed either regular rat chow (control animals) or a high-lipid rat chow with a high dose of vitamin D2 to induce atherosclerotic plaques. One milliliter of a cRGD-functionalized MS suspension (10^9 MSs mL^{-1}) labeled with approximately 500μCi of ^{64}Cu isotope was injected into each animal ($n = 3$) through the jugular vein and allowed to circulate for one hour. The injection was followed by *in vivo* PET-CT scanning, then *ex vivo* dark box imaging and gamma well counting of tissue specimens. Another group of animals ($n = 2$) was injected with non-targeted MSs to evaluate the non-specific binding.

2.7. Statistical analysis

For both the *in vitro* cell targeting study and the *in vivo* atherosclerotic plaque study, optical signals were measured across six different locations on the samples, and the average and standard deviation of the signal intensities were calculated. In addition, Student's t-tests were performed on all experimental data to determine the statistical significance, and to evaluate the difference in targeting efficiency between the targeted and the non-targeted MSs.

3. Results

3.1. Fabrication and characterization of ^{64}Cu-labeled QD-MSs

For the CL and CL-FL imaging in this study, QDs with an 800 nm emission peak were encapsulated in the vegetable oil core of the MSs. The BSA shell was labeled with ^{64}Cu isotope, a positron-emitting PET isotope that generates positrons with sufficient energy to produce CL (Dothager *et al* 2010, Ruggiero *et al* 2010). To demonstrate QD-MSs as a targeting agent, the BSA surface of MSs was modified through PEGylation to extend *in vivo* circulation time (Veronese and Pasut 2005, Madani *et al* 2007) (supplementary figure 1 stacks.iop.org/ PMB/60/020727/mmedia), and cyclic RGD peptide was attached to target the $\alpha_v\beta_3$ integrin overexpressed in atherosclerotic lesions (Hoshiga *et al* 1995, Winter *et al* 2003, Burtea *et al* 2008). The microstructure of these MSs is shown in the schematic (figure 1(*a*)), as well as in the scanning electron microscope (SEM, figure 1(*b*)) and transmission electron microscope (TEM, figure 1(*c*)) images. The average size of the MSs measured using a Coulter counter (Beckman Coulter, Inc.) was $1.52 \pm 1.07 \mu$m.

3.2. Dependence of CL intensity on refractive index

To illustrate the relationship between CL intensity and refractive index, and to verify that MSs do not alter the basic properties of CL published previously (Mitchell *et al* 2011), we prepared MSs composed of different types of hydrophobic liquid cores (without QDs): fluorocarbon (electronic fluid fluorinert FC-43, 3M), vegetable oil (Crisco, J.M. Smucker Co.), and wintergreen oil (methyl salicylate, Sigma-Aldrich) with refractive indices of 1.25, 1.46, and 1.54, respectively (Lide 2005). The three types of MSs were prepared at equal concentration, labeled with equal doses of ^{64}Cu (100μCi), and imaged for one minute using a commercial dark box (Stanford Photonics, Inc.) to measure CL luminescence intensity. The system
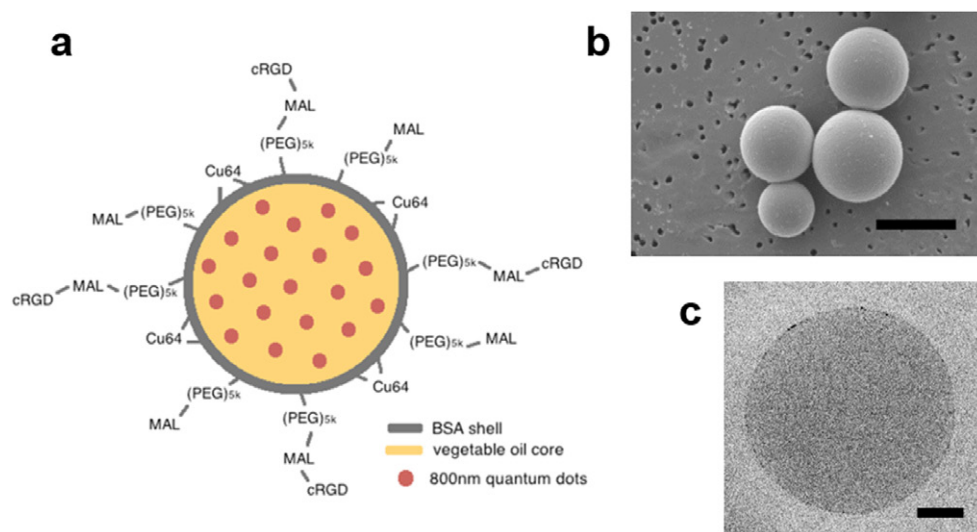
Figure 1. ^{64}Cu-labeled QD-MSs. (*a*) Schematic of a fully functionalized MS. [64]Cu isotope was conjugated directly to the BSA shell. PEG compounds were conjugated to the BSA shell through NHS-NH$_2$ reaction, and cRGD peptides were conjugated to the PEG compound through thiol-MAL reaction. (*b*) SEM image of MSs. (*c*) TEM image of a MS. Scale bars: (*b*) 2 μm; (*c*) 500 nm.

utilized a cooled (−21 °C) intensified CCD (iCCD) (XR Mega 10) with a selectable emission filter wheel. Figure 2(*a*) illustrates CL images of different MSs using a short pass (<500 nm) emission filter. Results show that at the same level of radioactivity, CL intensity from MSs with a vegetable oil core was approximately four-fold higher than from MSs with a fluoro-carbon core, and the CL intensity from MSs with a wintergreen oil core was approximately three-fold higher than from MSs with a vegetable oil core (figure 2(*b*)). Our experimental results can also be validated using equation (1), which clearly shows that a higher refractive index will increase the number of CL photons generated per distance dN/dx. This outcome is expected since dN/dx is directly proportional to $1 - 1/(\beta^2 n^2)$.

3.3. Wavelength-shifting of CL to NIR

With vegetable oil MSs, we further showed that the integration of NIR QDs increased the emission intensity at longer wavelengths. An optical emission intensity comparison study was performed between ^{64}Cu-labeled vegetable oil MSs with and without QDs. Samples were imaged using the luminescence dark box under both short pass (<500 nm) and long pass (>600 nm) emission filters for 1 min each. Optical signals detected under the short pass filter would predominantly be CL, since QDs have a narrow emission peak and would not be detected (Wu *et al* 2003, Smith *et al* 2008). Optical signals acquired under the long pass filter would include CL-excited QD fluorescence (CL-FL) and a small portion of CL due to its relatively weaker emission at longer wavelengths (Ruggiero *et al* 2010, Mitchell *et al* 2011). Dark box imaging confirmed that while MSs without QDs emitted a stronger signal intensity at shorter wavelengths, MSs with QDs emitted a much stronger intensity at longer wavelengths (figure 2(*c*)). We further investigated the difference in optical emission through tissue between ^{64}Cu-labeled QD MSs and ^{64}Cu in PBS at longer wavelengths, which served as a direct comparison between CL-FL from MSs and the commonly used pure CL from radioactive isotopes.
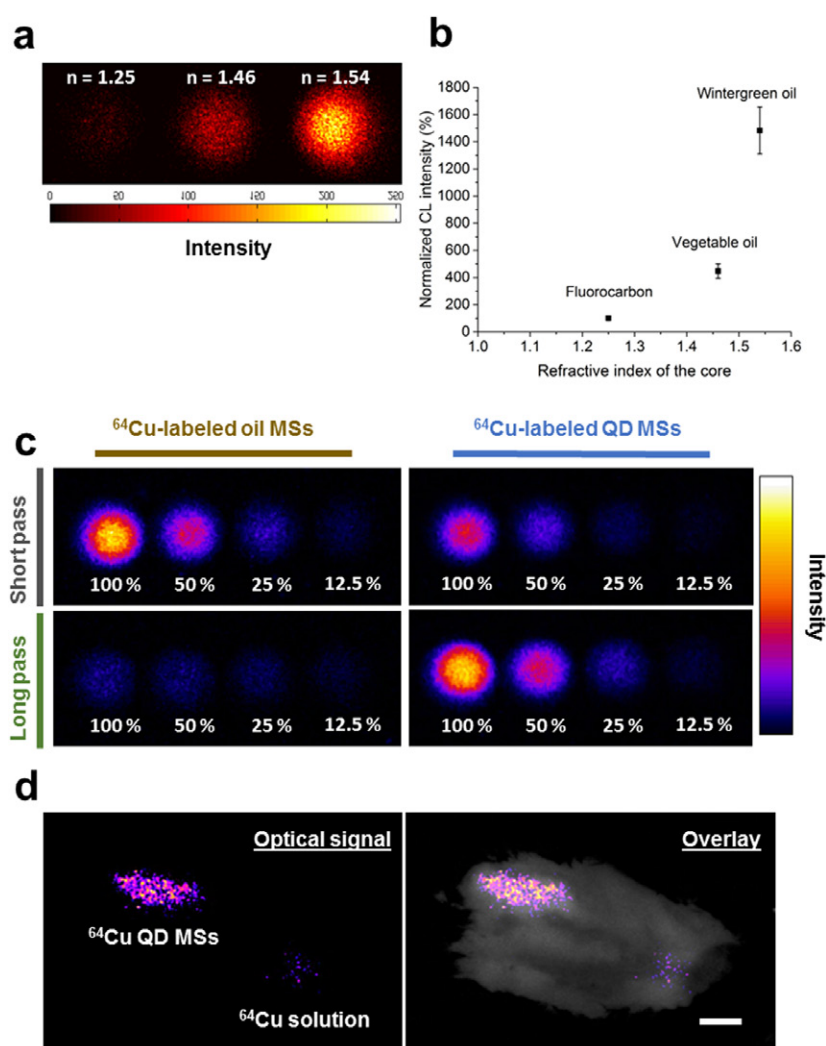
Figure 2. Characterization of CL and CL-excited QD fluorescence (CL-FL) using MSs. (*a*) CL emission intensity from MSs (10^7 MSs mL^{-1} for all three samples) with different core materials (without QDs) increases with higher core index. Left to right: fluorocarbon ($n = 1.25$), vegetable oil ($n = 1.46$), and wintergreen oil ($n = 1.54$). (*b*) CL emission comparison of the three types of MSs in (*a*) shows that MSs with higher index core yields higher signal intensity. (*c*) CL and CL-FL images of ^{64}Cu-labeled vegetable oil MSs and ^{64}Cu-labeled QD-MSs, respectively. ^{64}Cu-labeled oil MSs show stronger emission under a short pass filter (<500 nm) while ^{64}Cu-labeled QD-MSs show stronger emission under a long pass filter (>600 nm). Concentration (MSs/mL) in each image (left to right): 6×10^6 (100%); 3×10^6 (50%); 2×10^6 (25%); and 1×10^6 (12.5%). (*d*) Comparison of optical emission intensity through mouse skin between equal radiation doses of ^{64}Cu-labeled QD-MSs and ^{64}Cu solution shows stronger emission from the MSs under a long pass filter. Scale bar: (*d*) 1 cm.

The mouse for this experiment was injected subcutaneously with $200\,\mu$L ($20\,\mu$Ci) of each sample at different skin locations (figure 2(*d*)), and then imaged using the luminescence dark box. We observed an approximately four-fold higher optical emission from the MSs.

3.4. In vitro cell targeting

[64]Cu-labeled QD-MSs were tested for *in vitro* targeting of $\alpha_v\beta_3$ integrin to demonstrate the capability of these MSs as a targeting agent. We chose this specific integrin receptor based on previous successful targeting results using the same MSs (Toublan *et al* 2006). Quantum dot-MSs were functionalized with cRGD peptide, and human umbilical vein endothelial cells (HUVEC) were used, since this cell line is known to express $\alpha_v\beta_3$ integrin (Sriramarao *et al* 1993). Three experimental groups were tested: a control group with PBS solution, a targeted group with cRGD-functionalized MSs, and a non-targeted group with non-functionalized MSs to evaluate for any nonspecific binding. The three groups of cells were subsequently imaged using a fluorescence microscope (Axiovert 200, Zeiss), and targeting efficiency was determined based on average fluorescence intensity (figures 3(*a*)–(*c*)).

The cell study revealed an approximately three-fold higher binding of cRGD-functionalized MSs than the non-specific binding by the non-functionalized MSs ($p < 0.001$, figure 3(*d*)). In addition, we observed clusters of MSs adhering to the HUVEC cells in the targeted group (figure 3(*a*)). These clusters contributed to the saturating fluorescence signals seen in the corresponding fluorescence image. A more diffuse fluorescence, most likely from endocytosed or degraded MSs, was also observed in the cytoplasm of these cells, which was not attributed to autofluorescence, given the absence of autofluorescence in the control sample (figure 3(*c*)). Additional cell studies were also conducted using human breast cancer cell lines to further determine the targeting specificity of the functionalized MSs (supplementary figure 2 stacks. iop.org/PMB/60/020727/mmedia).

3.5. In vivo targeting and ex vivo CL-FL imaging of atherosclerotic plaques

To examine the targeting efficiency of ^{64}Cu-labeled cRGD-functionalized PEGylated QD-MSs as a potential *in vivo* targeting agent and the potential use of CL imaging for disease detection, we performed a proof-of-concept study of *in vivo* targeting of atherosclerotic plaques in a hyperlipidemic rodent model. Atherosclerosis was selected as a disease model since we had previously demonstrated *ex vivo* targeting of atherosclerotic plaques using MSs (Kim *et al* 2014). The spatial distribution of MSs and the CL-FL was assessed *in vivo* using a microPET-CT scanner (Inveon, Siemens Healthcare) and *ex vivo* in the excised rat aortas using the luminescence dark box. Biodistribution of MSs was also examined with post-mortem gamma well counting.

In vivo PET-CT showed scattered PET signals around the aortic arch after one hour of MS circulation (figure 4(*a*); red arrows). The animals were then euthanized, and their aortas were excised for CL-FL imaging. Excised tissue was imaged for five minutes under the long pass emission filter, and CL-FL signal was observed primarily from the aortic arch and thoracic aorta (figure 4(*b*)). To verify the CL-FL signal, the same segment of aorta was also imaged using a fluorescence dark box (Maestro, CRi, Inc.) equipped with a 445–490 nm excitation filter and an 800 nm long-pass emission filter. The locations of signal were relatively consistent with the results from CL-FL imaging (figure 4(*c*)), with slight differences due to re-positioning of the aortas and different sensitivity levels between the two systems. In addition to optical imaging, the same aorta segments, along with blood and skin samples, were analyzed with a gamma well counter (Wizard2, Perkin Elmer) to directly measure the radioactivity in the tissue specimens. Data confirmed that the aorta had higher radioactivity levels than blood and skin, and the aortic arch showed higher activity levels than the thoracic aorta segment (figure 4(*d*) stacks.iop.org/PMB/60/020727/mmedia). These findings were consistent with the optical imaging results.
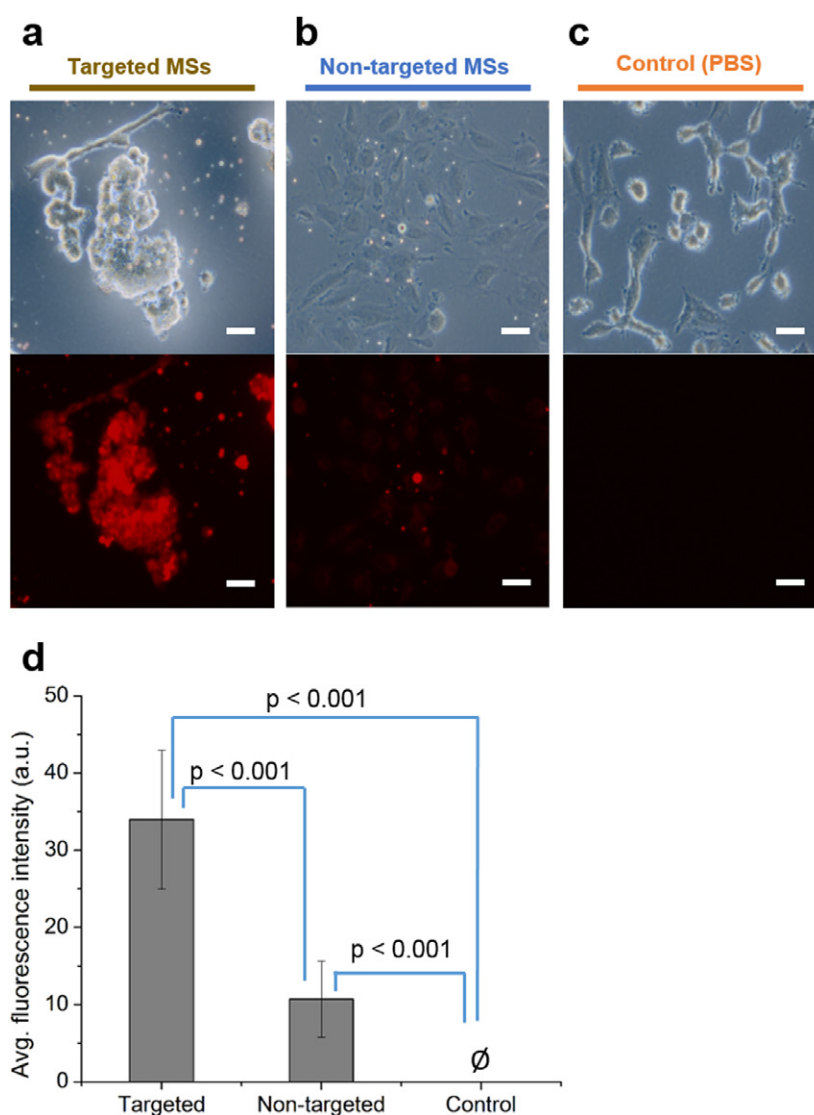
Figure 3. *In vitro* study with HUVEC cells shows significantly higher specific binding of cRGD-functionalized MSs than non-specific binding of MSs without cRGD. Bright field: top; fluorescence: bottom. (*a*) Targeted group with cRGD-functionalized MSs. (*b*) Non-targeted group with non-functionalized MSs. (*c*) Control group treated with PBS solution. (*d*) Comparison of fluorescence intensity from the three groups of cells shows approximately three-fold higher fluorescence intensity from the targeted group than from the non-targeted group. All values are expressed as mean ± SD ($n = 4$/group). Scale bar: 40 μm, applies to all images.

The *in vivo* study was also repeated using non-functionalized MSs to evaluate *in vivo* targeting efficiency. CL-FL imaging of excised aorta showed low optical signal intensity (supplementary figure 3(*a*) stacks.iop.org/PMB/60/020727/mmedia). Furthermore, the same aorta revealed weak QD fluorescence during subsequent fluorescence imaging (supplementary figure 3(*b*) stacks.iop.org/PMB/60/020727/mmedia). Average CL-FL intensity emitted from the
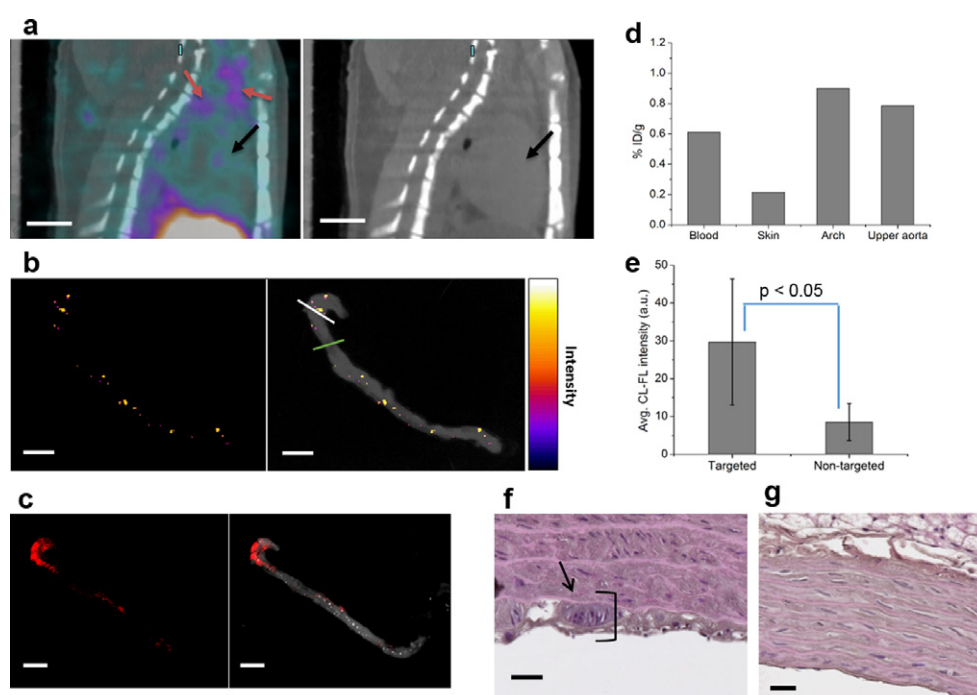
Figure 4. *In vivo* targeting of cRGD-functionalized MSs and imaging of atherosclerotic lesions. (*a*) *In vivo* sagittal PET-CT (left) and CT (right) scans show binding of MSs on the aortic arch. Black arrows: heart; red arrows: PET signals localized to the aortic arch. (*b*) CL-FL images of the excised aorta showing optical signals from the aortic arch and various other locations along the aorta. Histology section locations are indicated by the white and green lines in the composite (CL-FL plus bright field) image. Left: CL-FL signals; right: composite image. (*c*) QD fluorescence image of the same aorta in (*b*), showing fluorescence from the aortic arch and the thoracic aorta. Left: fluorescence; right: composite image. (*d*) Biodistribution of the targeted MSs based on gamma well counter data from post-mortem specimens illustrates the higher level of radioactivity in the aorta compared to that in the blood, which is consistent with the dark box images. (*e*) The signal intensity from the targeted study is approximately three-fold higher than that from the non-targeted study. (*f*) Histology section from the location specified by the white line in (*b*). Thickening of the aorta and evidence of fibrous plaque is indicated. (*g*) Histology section from the location specified by the green line in (*b*), which appears normal. Scale bars: (*a*) 1 cm; (*b-c*) 5 mm; (*f-g*) 25 μm.

aortas with targeted and non-targeted MSs was measured. Signal intensity from the targeted MSs was approximately three-fold higher than that from the non-targeted MSs ($p < 0.05$, figure 4(*e*)).

3.6. Histology validation

To validate the imaging results and the presence of disease, histology was performed at different locations on the aorta, including the arch, where optical signals were obtained (figure 4(*b*), white line), and at a location on the thoracic aorta where no optical signal was detected (figure 4(*b*), green line). The hematoxylin and eosin (H & E)-stained histology sections were examined by a board-certified pathologist 'blinded' to the imaging results. Analysis confirmed that

the histology sections from the aortic arch showed signs of early-stage fibrous plaques (Figure 4(*f*)) which contain collagen fibers (Bloom and Fawcett 1975, Wheater *et al* 1991). Thickening of the *tunica intima* with accumulation of foam cells was also observed in this region, which is typical for atherosclerosis (Wheater *et al* 1991). In contrast, these physiological characteristics were not observed in histology sections from regions of the thoracic aorta where no optical signals were evident (figure 4(*g*)). The tissue from this region appeared normal without thickening of the vessel wall. The histology sections of the aorta from the non-targeted study were also examined, and optical signals were not detected at histological sites where plaques were observed (supplementary figure 3(*c*) stacks.iop.org/PMB/60/020727/mmedia).

4. Discussion

The development of CL imaging has rapidly progressed since its first application in biomedical imaging, and quantitative characterization and disease screening using this technology, including clinical studies, have been demonstrated by various research groups (Spinelli *et al* 2013, Thorek *et al* 2014). However, practical challenges for CL imaging still exist. Due to the short-wavelength emission of CL, current applications are mainly limited to tumors or thyroid diseases that are located closer to the skin surface (Ruggiero *et al* 2010, Spinelli *et al* 2013, Thorek *et al* 2014). While the combination of QDs with CL-emitting radioisotopes have been shown to shift CL emission toward longer-wavelengths, the amount of improvement in tissue penetration depth and signal intensity can be limited by the weak intensity of CL, which is attributed to the inefficient conversion process of β-particle energy to Cerenkov light (Mitchell *et al* 2011). In our study, we have attempted to address this challenge by intensifying the CL used for QD excitation by altering the refractive index of the local medium where the CL is generated, named inside the core of the MSs.

Previous studies have shown that protein-shell oil-core MSs can be fabricated and modified for use in a variety of imaging modalities, including ultrasound imaging, magnetic resonance imaging (MRI), fluorescence imaging, and magnetomotive optical coherence tomography (MM-OCT) (John *et al* 2012, Kim *et al* 2014). In this study, we further modified the MSs to serve as an agent that is capable of enhancing and converting CL emission toward the NIR. We demonstrated that our MSs successfully enhanced the CL emission from ^{64}Cu isotopes by four-fold, indicating that CL emission can be intensified by increasing the refractive index of the MS core. Our results in mouse skin suggest that utilizing both a high-index oil core ($n = 1.46$), which is greater than the average refractive index of tissue ($n = 1.38$) (Tearney *et al* 1995), and the QDs increases optical emission intensity through the skin at longer wavelengths, and can potentially improve CL imaging of deeper tissue.

In addition, our *in vitro* and *in vivo* findings demonstrated that ^{64}Cu-labeled QD MSs can be utilized as a multimodal imaging contrast agent for disease targeting, such as targeting of atherosclerotic plaques. *Ex vivo* CL-FL imaging of the excised aortas showed that the targeted QD-MSs have a significantly higher level of binding compared to the non-targeted MSs, which was validated by *in vivo* PET-CT scanning, *ex vivo* fluorescence imaging, and histology. The correlation among all imaging results suggests that CL imaging can be a reliable screening tool.

5. Conclusion

In conclusion, we have successfully fabricated radiolabeled protein-shell oil-core MSs that encapsulate QDs for CL-FL imaging. The unique and versatile design of these MSs can be readily modified for enhancing contrast signals in different imaging modalities, and the

relatively large volume of the MS core offers the potential for use as a drug delivery capsule. In addition to the application employed in our study, these MSs together with CL imaging could be used as diagnostic tools for a variety of diseases, including cancer. This engineered and fabricated design that combines the advantages of a high-refractive-index core medium and the wavelength-shifting CL-FL technique has potential for *in vivo* CL imaging.

Further development of this imaging technology is needed to demonstrate clinical potential, such as the construction and use of an intravascular or intra-luminal catheter for CL imaging. Moreover, additional *in vivo* experiments are needed to evaluate and optimize the performance of the current MS contrast agent design to achieve better signal generation and contrast. Our study contributes to a growing number of investigations that continue to demonstrate the potential of CL imaging for biomedical applications.

Acknowledgments

Competing financial interests

S A B is co-founder of Diagnostic Photonics, Inc., which is licensing intellectual property from the University of Illinois at Urbana-Champaign related to Interferometric Synthetic Aperture Microscopy. S A B receives patent royalties from the Massachusetts Institute of Technology for technology related to optical coherence tomography. Other authors declare no competing financial interests.

References

Bloom W and Fawcett D 1975 *A Text Book of Histology* (Philadelphia, PA: W B Saunders Company)

Boschi F and Spinelli A E 2012 Quantum dots excitation using pure beta minus radioisotopes emitting Cerenkov radiation *R. Soc. Chem. Adv.* **2** 11049–52

Burtea C, Laurent S, Murariu O, Rattat D, Toubeau G, Verbruggen A, Vansthertem D, Elst L V and Muller R N 2008 Molecular imaging of avb3 integrin expression in atherosclerotic plaques with a mimetic of RGD peptide grafted to Gd-DTPA *Cardiovasc. Res.* **78** 148–57

Dobrucki L W and Sinusas A J 2010 PET and SPECT in cardiovascular molecular imaging *Nat. Rev. Cardiol.* **7** 38–47

Dothager R S, Goiffon R J, Jackson E, Harpstrite S and Piwnica-Worms D 2010 Cerenkov radiation energy transfer (CRET) imaging: a novel method for optical imaging of PET isotopes in biological systems *PLoS One* **5** e13300

Hoshiga M, Alpers C E, Smith L L, Giachelli C M and Schwartz S M 1995 $\alpha_v\beta_3$ integrin expression in normal and atherosclerotic artery *Circ. Res.* **77** 1129–35

Jackson T, Sharma A, Ghazaleh R A, Blakemore W E, Ellard F M, Simmons D L, Newman J W, Stuart D I and King A M 1997 Arginine–glycine–aspartic acid-specific binding by foot-and-mouth disease viruses to the purified integrin $\alpha_v\beta_3$ *in vitro J. Virol.* **71** 8357–61

Jelley J V 1955 Cerenkov radiation and its applications *Br. J. Appl. Phys.* **6** 227

John R, Nguyen F T, Kolbeck K J, Chaney E J, Marjanovic M, Suslick K S and Boppart S A 2012 Targeted multifunctional multimodal protein-shell microspheres as cancer imaging contrast agents *Mol. Imaging Biol.* **14** 17–24

Kim J, Ahmad A, Marjanovic M, Chaney E J, Li J, Rasio J, Hubler Z, Spillman D, Suslick K S and Boppart S A 2014 Magnetomotive optical coherence tomography for the assessment of atherosclerotic lesions using $\alpha_v\beta_3$ integrin-targeted microspheres *Mol. Imaging Biol.* **16** 36–43

Lide D R (ed) 2005 *CRC Handbook of Chemistry and Physics* (Boca Raton, FL: CRC)

Liu H G, Carpenter C M, Jiang H, Pratx G, Sun C, Buchin M P, Gambhir S S, Xing L and Cheng Z 2012 Intraoperative imaging of tumors using Cerenkov luminescence endoscopy: a feasibility experimental study *J. Nucl. Med.* **53** 1579–84

Liu H G, Zhang X F, Xing B G, Han P Z, Gambhir S S and Cheng Z 2010 Radiation-luminescence-excited quantum dots for *in vivo* multiplexed optical imaging *Small* **6** 1087–91

Madani F, Bessodes M, Lakrouf A, Vauthier C, Scherman D and Chaumeil J C 2007 PEGylation of microspheres for therapeutic embolization: preparation, characterization and biological performance evaluation *Biomaterials* **28** 1198–208

Mitchell G S, Gill R K, Boucher D L, Li C Q and Cherry S R 2011 *In vivo* Cerenkov luminescence imaging: a new tool for molecular imaging *Phil. Trans. R. Soc. A* **369** 4605–19

Peterson G L 1977 A simplification of the protein assay method of Lowry *et al* which is more generally applicable *Anal. Biochem.* **83** 346–56

Robertson R, Germanos M S, Li C, Mitchell G S, Cherry S R and Silva M D 2009 Optical imaging of Cerenkov light generation from positron-emitting radiotracers *Phys. Med. Biol.* **54** N355–65

Ruggiero A, Holland J P, Lewis J S and Grimm J 2010 Cerenkov luminescence imaging of medical isotopes *J. Nucl. Med.* **51** 1123–30

Smith A M, Duan H W, Mohs A M and Nie S M 2008 Bioconjugated quantum dots for *in vivo* molecular and cellular imaging *Adv. Drug Deliv. Rev.* **60** 1226–40

Spinelli A E, Ferdeghini M, Cavedon C, Zivelonghi E, Calandrino R, Fenzi A, Sbarbati A and Boschi F 2013 First human Cerenkography *J. Biomed. Opt.* **18** 020502

Sriramarao P, Mendler M and Bourdon M A 1993 Endothelial-cell attachment and spreading on human tenascin is mediated by $\alpha_2\beta_1$ and $\alpha_v\beta_3$ integrins *J. Cell Sci.* **105** 1001–12

Tearney G J, Brezinski M E, Southern J F, Bouma B E, Hee M R and Fujimoto J G 1995 Determination of the refractive-index of highly scattering human tissue by optical coherence tomography *Opt. Lett.* **20** 2258–60

Thorek D L J, Robertson R, Bacchus W A, Hahn J, Rothberg J, Beattie B J and Grimm J 2012 Cerenkov imaging—a new modality for molecular imaging *Am. J. Nucl. Med. Mol. Imaging* **2** 163–73 (PMCID: PMC3477724)

Thorek D L J, Riedl C C and Grimm J 2014 Clinical Cerenkov luminescence imaging of ^{18}F-FDG *J. Nucl. Med.* **55** 95–8

Toublan F J J, Boppart S and Suslick K S 2006 Tumor targeting by surface-modified protein microspheres *J. Am. Chem. Soc.* **128** 3472–3

Veronese F M and Pasut G 2005 PEGylation, successful approach to drug delivery *Drug Discov. Today* **10** 1451–8

Weissleder R and Pittet M J 2008 Imaging in the era of molecular oncology *Nature* **452** 580–9

Wheater P, Burkitt H, Stevens A and Lowe J 1991 *Basic Histopathology* (New York: Churchill Livingstone)

Winter P M *et al* 2003 Molecular imaging of angiogenesis in early-stage atherosclerosis with $\alpha_v\beta_3$-integrin-targeted nanoparticles *Circulation* **108** 2270–4

Wu X Y, Liu H J, Liu J Q, Haley K N, Treadway J A, Larson J P, Ge N F, Peale F and Bruchez M P 2003 Immunofluorescent labeling of cancer marker Her2 and other cellular targets with semiconductor quantum dots *Nat. Biotechnol.* **21** 41–6

Xu Y D, Chang E, Liu H G, Jiang H, Gambhir S S and Cheng Z 2012 Proof-of-concept study of monitoring cancer drug therapy with Cerenkov luminescence imaging *J. Nucl. Med.* **53** 312–7

Xu Y D, Liu H G and Cheng Z 2011 Harnessing the power of radionuclides for optical imaging: Cerenkov luminescence imaging *J. Nucl. Med.* **52** 2009–18